Available online at www.sciencedirect.com

ScienceDirect

journal homepage: www.elsevier.com/locate/he

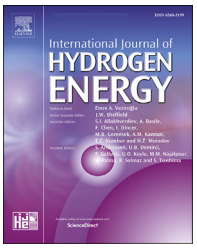

Short Communication

Insight into hydrogen effect on a duplex medium-Mn steel revealed by in-situ nanoindentation test

X. Lu [a,*], Y. Ma [b], M. Zamanzade [c], Y. Deng [a], D. Wang [a], W. Bleck [b], W.W. Song [b,**], A. Barnoush [a]

[a] Department of Mechanical and Industrial Engineering, Norwegian University of Science and Technology, No-7491 Trondheim, Norway

[b] Steel Institute (IEHK), RWTH Aachen University, D-52072 Aachen, Germany

[c] Department of Materials Science, Saarland University, D-66041 Saarbrücken, Germany

HIGHLIGHTS

- Hydrogen effect on a duplex medium-Mn steel was studied by nanoindentation test.
- Hydrogen impact on nanomechanical response of each component was reported.
- A reduction of stacking fault energy (SFE) was observed in the hydrogen environment.
- Hydrogen leads to a suppression of retained austenite to α′-martensite transformation.

ARTICLE INFO

Article history:
Received 6 December 2018
Received in revised form
18 March 2019
Accepted 23 April 2019
Available online xxx

Keywords:
Medium-Mn steel
Nanoindentation
Deformation induced martensite transformation
Hydrogen embrittlement

ABSTRACT

Medium-Mn steel is the newly developed steel acting as a promising candidate of the 3rd-generation advanced high strength steels. In the present study, the effect of hydrogen on the mechanical behavior and martensite transformation process in a duplex medium-Mn steel is investigated by in-situ nanoindentation test. The mechanical response of individual phase: ferrite, and retained austenite by introducing hydrogen is studied. With the presence of hydrogen, the reduction of activation energy for dislocation nucleation was verified by using a stress-biased, statistical thermal activation model. The stacking fault energy (SFE) was reduced, which was revealed by electron channeling contrast (ECC) technique. Magnetic force microscopy (MFM) revealed a suppression of retained austenite to α′-martensite transformation with the presence of hydrogen, which is related to hydrogen induced SFE reduction and enhanced slip planarity.

* *Corresponding author*. Department of Mechanical and Industrial Engineering (MTP), Norwegian University of Science and Technology (NTNU), Richard Birkelandsvei 2B, NO-7491 Trondheim, Norway.

** *Corresponding author*. Steel Institute (IEHK), RWTH Aachen University, Intzestr. 1, D-52072 Aachen, Germany.

E-mail addresses: xu.lu@ntnu.no (X. Lu), wenwen.song@iehk.rwth-aachen.de (W.W. Song).

https://doi.org/10.1016/j.ijhydene.2019.04.290

Introduction

Aiming at increasing safety and fuel economy, advanced high strength steels (AHSS) were developed to meet the demand for industries like automotive and aerospace. As one of the promising candidate of the 3rd-generation AHSS, medium-Mn steels (MMnS, Mn $\leq$ 12 wt %) become popular due to the combination of high strength and ductility [1,2]. By choosing a proper intercritical annealing temperature, one is able to get an ultrafine-grained (UFG) duplex microstructure consisting of retained austenite (γ_R) and ferrite (α) [3–5]. Due to a relatively low stacking fault energy (SFE) of retained austenite, both twinning-induced-plasticity (TWIP) and transformation-induced-plasticity (TRIP) mechanisms can be triggered during plastic deformation [6]. Researchers have been focusing on improving the mechanical properties [7,8] and understanding the microstructure evolution during deformation for years [9–11]. However, along with the exploitation of such high-strength steels [9,10], hydrogen embrittlement (HE) becomes a severe problem that one should focus on [12,13]. Hydrogen-induced pre-mature failure has been a hot topic with the common feature of transforming ductile to brittle fracture [14–17]. In MMnS, however, the complexity of microstructure (multiphase, UFG structure and metastable phase *etc.*) generates difficulties in understanding the HE phenomenon [18–20]. And the effect of hydrogen on MMnS is rarely reported. Nevertheless, understanding the hydrogen effects on individual constitutive components is, in particular, of great importance to disentangle HE mechanisms in multiphase steels. As a fast and flexible nanomechanical testing tool, nanoindentation can be used to quantify the mechanical properties of separate phases at microscale [21–24]. Moreover, the introduction of in-situ electrochemical nanoindentation (ECNI) gives the possibility of a real-time study of the effect of hydrogen [25,26]. In this work, ECNI test was performed as a very first attempt to shed new light on the hydrogen susceptibility of individual phase components in MMnS.

Experimental

The chemical composition of the studied steel is Fe-12Mn-3Al-0.05C (wt. %). The steel was produced from a cast ingot, followed by a sequence of hot rolling, homogenization, austenitization, cold rolling, and intercritical annealing at 700 °C for 12 h. Details of the processing can be found in Ref. [27]. Initial phase information was investigated by high-energy synchrotron X-ray diffraction (SYXRD) at a fixed energy of ~60 keV and a corresponding wavelength of 0.20738 Å. The SYXRD pattern was analyzed by Rietveld refinement method using software MAUD [28]. Before testing, the sample was prepared to electropolishing level in a methanolic H_2SO_4 solution. The ECNI test was done with Hysitron TI950 TriboIndenter integrated with a three-electrode electrochemical setup [26,29]. A Berkovich tip with a half angle of 65.3° was used inside the electrolyte designed for hydrogen charging, which is a glycerol-based borax solution containing 0.002 mol/L $Na_2S_2O_3$ to promote hydrogen absorption. The electrolyte can preserve the surface integrity by keeping the surface roughness down to several nanometers [30]. The sample was charged at −1600 $mV_{/Hg/HgSO4}$ for hydrogen adsorption. Two hours pre-charging was guaranteed and the surface topography was continuously checked with the same tip used for nanoindentation. The load function was designed with a maximum load of 1500 μN and an 8000 μNs^{-1} loading rate to eliminate the influence of fluctuation induced by hydrogen charging. At least 40 indents were performed in each phase with and without hydrogen. The postmortem microstructure analysis on the indents was performed using high-resolution scanning electron microscopy (SEM, Quanta FEG 650 ESEM, FEI Inc.) with electron channeling contrast (ECC) technique. Electron backscatter diffraction (EBSD) was used to help eliminate the indents that were made on phase boundaries. A magnetic probe embedded in the atomic force microscope (AFM) was applied to characterize the phase transformation during the test.

Results and discussion

Fig. 1 (a) shows the initial microstructure of the studied material, which consists of α and γ_R. Due to a relatively high intercritical annealing temperature and sufficient annealing time, the microstructure was fully recrystallized from cold-rolled martensite, resulting in the equiaxed morphology of grains. Inverse pole figure (IPF) and phase distribution obtained from EBSD (Fig. 1 (b) and (c)) show UFG α and γ_R with the average grain size of 1.19 μm and 1.28 μm, respectively. The volume fraction of austenite is 61.3% based on the SYXRD result, as is shown in Fig. 1 (d). In contrast to the other work showing both upper and lower yield stress with a large Lüders strain [10,31,32], the engineering stress-strain curve of the studied material tested in air at a strain rate of 10^{-3} s^{-1} exhibits a continues yielding and pronounced strain hardening as presented in Fig. 1 (e). The present material shows a yield strength ($R_{p0.2}$) of 444.3 MPa, ultimate tensile strength (R_m) of 824.0 MPa and a total elongation (A_{20}) of 32.6%. Besides, it is confirmed that the studied material contains metastable austenite with a SFE of 11 mJ/m^2, which is lower than the value for TRIP-TWIP transition, therefore the TRIP effect dominates during deformation [27].

Hydrogen effect on pop-in behavior

ECNI tests were performed on defined phases and the corresponding load-displacement (P-h) curves are presented in the cases of air and hydrogen in Fig. 2 (a)-(b). Two representative curves in each condition are shown in Fig. 2 (d)-(e). In the case of α, each of the P-h curves shows a single distinguished pop-in, which corresponds to the onset of plasticity starting from dislocation nucleation in the defect-free lattice [25,26,33–35]. In the present study, all of the P-h data showed a clear pop-in, which indicates a fully recrystallization process with a relatively low dislocation density in our material. Similar results showing pop-ins in recrystallized grains were also reported on another specially designed MMnS (Fe-7.16Mn-0.14C-0.23Si, wt. %) [10]. When hydrogen is introduced, P-h curves obtained from α show decrease or vanish in the pop-in load (from 234.6 ± 69.8 to 96.46 ± 87.1 μN) and width (Fig. 2 (d)), and this phenomenon has already been reported on aluminum, Fe-Al

Please cite this article as: Lu X et al., Insight into hydrogen effect on a duplex medium-Mn steel revealed by in-situ nanoindentation test, International Journal of Hydrogen Energy, https://doi.org/10.1016/j.ijhydene.2019.04.290

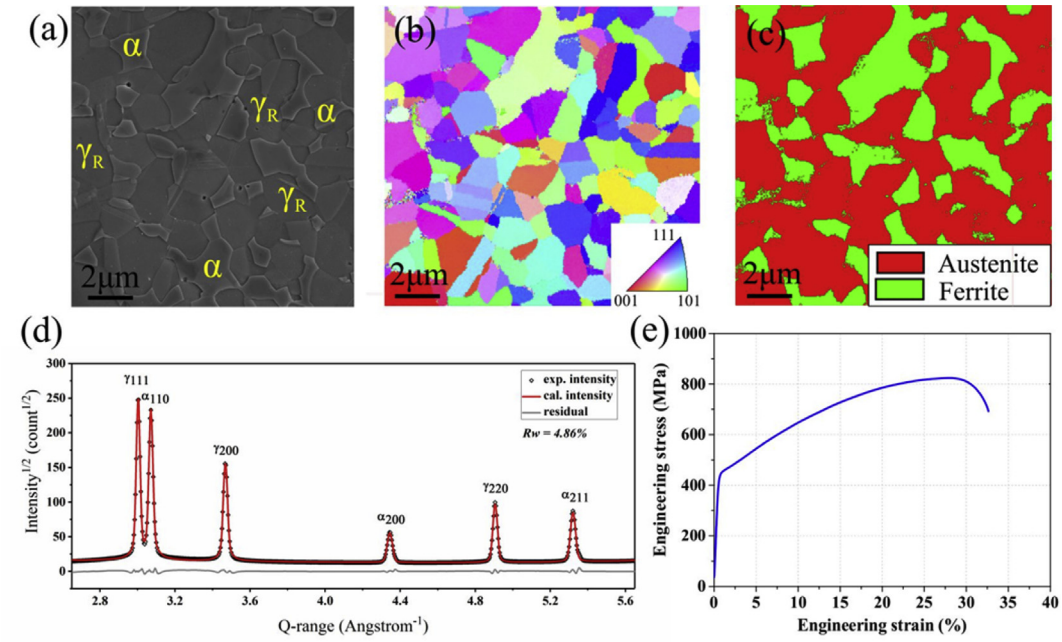

Fig. 1 – (a) SEM image showing initial microstructure of the MMnS: ferrite (α) and retained austenite (γ_R); (b)–(c): corresponding IPF and phase images obtained from EBSD, step size 45 nm; (d) SYXRD profiles of the present MMnS; and (e) Engineering stress-strain curve obtained in air at constant strain rate of 10^{-3} s^{-1}.

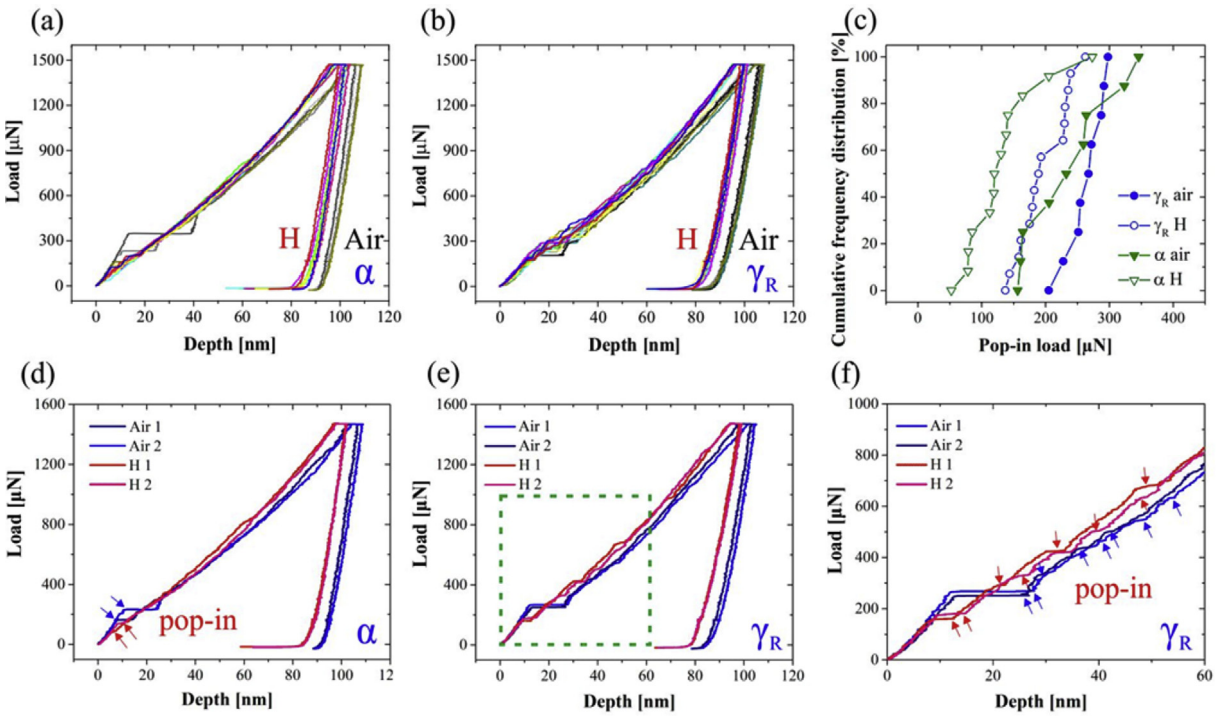

Fig. 2 – (a)–(b) Nanoindentation P-h curves for α and γ_R tested with and without hydrogen; (c) cumulative frequency distribution of pop-in loads for indentation tests with and without hydrogen; (d)–(e) Representative curves for each phase showing the influence of hydrogen on pop-in behavior; (f) enlarged view of the highlighted green area in (e). (For interpretation of the references to color in this figure legend, the reader is referred to the web version of this article.)

intermetallic and Ni-base superalloy [26,29]. The reduction in activation energy for dislocation nucleation by introducing hydrogen was proposed to be the reason [26]. In contrast in the air condition, P-h curves of γ_R show multiple pop-in behaviors (Fig. 2 (e)-(f)), where the first pop-in relates to the plasticity initiation by dislocation and subsequent pop-ins were confirmed to be the body-centered tetragonal (bct) α′-martensite formation [10,36,37]. The same trend for the first

Please cite this article as: Lu X et al., Insight into hydrogen effect on a duplex medium-Mn steel revealed by in-situ nanoindentation test, International Journal of Hydrogen Energy, https://doi.org/10.1016/j.ijhydene.2019.04.290

pop-in load as in α is observed here by hydrogen ingression. The corresponding cumulative distributions, f, of first pop-in loads in each condition are illustrated in Fig. 2 (c). The scattering of the pop-in loads (Fig. 2 (c)) is a common feature due to the dislocation nucleation process, which relates to the thermal contribution and local stress variations below the tip.

The activation energy for dislocation nucleation can be fitted by a stress-biased, statistical thermal activation model describing the incipient plasticity suggested by Schuh et al. [38,39]. The nucleation rate per unit volume of material can be expressed as:

$$\dot{N} = N_0 \cdot \exp\left(-\frac{\varepsilon - \tau_{max} \upsilon^*}{kT}\right) \quad (1)$$

where N_0 is a pre-exponential frequency parameter. ε is the activation energy required for the dislocation nucleation, which can be reduced by mechanical work and thermal energy kT (k is the Boltzmann constant, T is the temperature). The mechanical work equals to the maximum shear stress τ_{max} acting on an activation volume υ^*. Furthermore, the statistic representation of the first pop-in behavior at a constant loading (stress) rate $\dot{\tau}$, can be described as [38]:

$$f = 1 - \exp\left[-N_0 \cdot \exp\left(-\frac{\varepsilon}{kT}\right) \cdot \frac{kT}{\dot{\tau}\upsilon^*} \cdot \exp\left(\frac{\tau_{max}\upsilon^*}{kT}\right)\right] \quad (2)$$

By plotting $ln[\ln(1-f)^{-1}]$ versus τ_{max}, υ^* in each condition can therefore be extracted by using a linear least-squares fitting method. τ_{max} relates to the pop-in load P_{pop-in}:

$$\tau_{max} = 0.31\left(\frac{6E_r^2}{\pi^3 R^2} P_{pop-in}\right) \quad (3)$$

where E_r is the reduced elastic modulus that can be predicted by using Hertzian law in the earliest elastic stage [40]:

$$P = \frac{4}{3} E_r \sqrt{Rh^3} \quad (4)$$

where P is the applied load, and h is the indentation depth. The tip curvature radius R was unambiguously determined to be 828.3 nm by indenting on a standard fused quartz with elastic modulus of 69.6 GPa. The fitting of reformulated Eq. (2) is shown in Fig. 3 (a), where υ^* are represented by the slope of the plots. υ^* for γ_R is in the order of 2 Ω (Ω is the atomic volume, Ω = 0.25a^3, a is lattice parameter of 3.62 Å obtained from SYXRD) with 5.09% expansion in hydrogen case. And υ^* for α has an increment of 9.81% with the values of ~2.5 Ω (a = 2.89 Å). However, $\tau_{max}\upsilon^*$ shows an average reduction of 5.31% for γ_R, and 13.33% for α. On one hand, these results are in line with the proposed mechanism: at a constant temperature, the lowering of the activation energy for dislocation nucleation by having hydrogen in the system reduces the necessary mechanical work for overcoming the energy barrier. On the other hand, recently reported ex-situ nanoindentation test on a high-entropy alloy showed that activation volume doubles by introducing hydrogen, which was explained by the vacancy-mediated heterogeneous dislocation nucleation involving the motion of several atoms [41]. In contrast, the activation volume for nucleation in presence of hydrogen in the current study only shows marginal increment. The inconsistency of our results to Ref. [41] elucidates no noticeable vacancies were induced by hydrogen, and the main contribution of hydrogen to plasticity onset resides in lowering the activation energy for dislocation nucleation.

Hydrogen effect on nanohardness

Besides, the nanohardness variation obtained by the maximum applied load P_{max}/A_c is shown in Fig. 3 (b). Both γ_R and α show an increment with hydrogen from 3.68 ± 0.09 to 4.04 ± 0.08 GPa, and 3.62 ± 0.09 to 3.76 ± 0.19 GPa, respectively. The hardness increment on Ni-base superalloy [29], austenitic stainless steel [42], and super duplex stainless steel (SDSS) [43] was explained through the stress state alteration by the presence of hydrogen [26]. Besides, lattice friction increment due to short-range interactions between dislocations and hydrogen atoms was also proposed as a reason [44]. The hardening effect is more intense in γ_R, which can also be related to its higher solubility of hydrogen. Indisputably, hardness variation could also attribute to their different composition due to partitioning of alloying elements in γ_R and α [4]. Controversial results showing hardening to softening transition with different charging parameters and testing methods were also reported [45,46], wherein they claimed the indenter geometry and the hydrogen concentration to be the

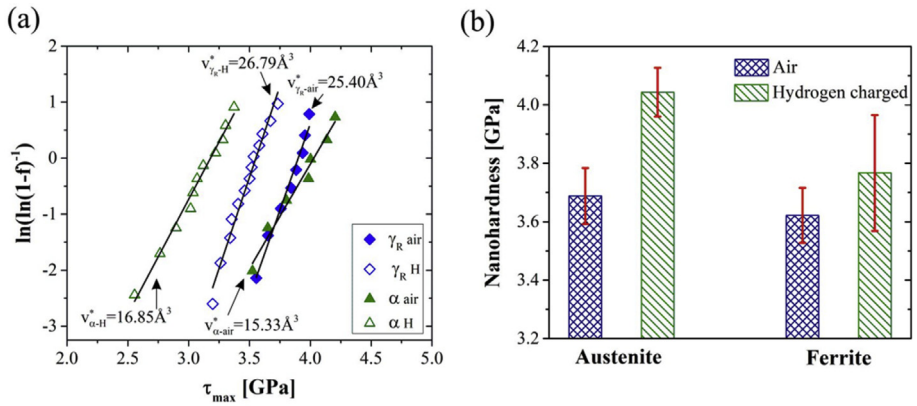

Fig. 3 – (a) Linear least-squares fitting of the reformulated Eq. (2), excluding the tails of the distribution; the impact of hydrogen on nanohardness (b) of austenite and ferrite phases.

Please cite this article as: Lu X et al., Insight into hydrogen effect on a duplex medium-Mn steel revealed by in-situ nanoindentation test, International Journal of Hydrogen Energy, https://doi.org/10.1016/j.ijhydene.2019.04.290

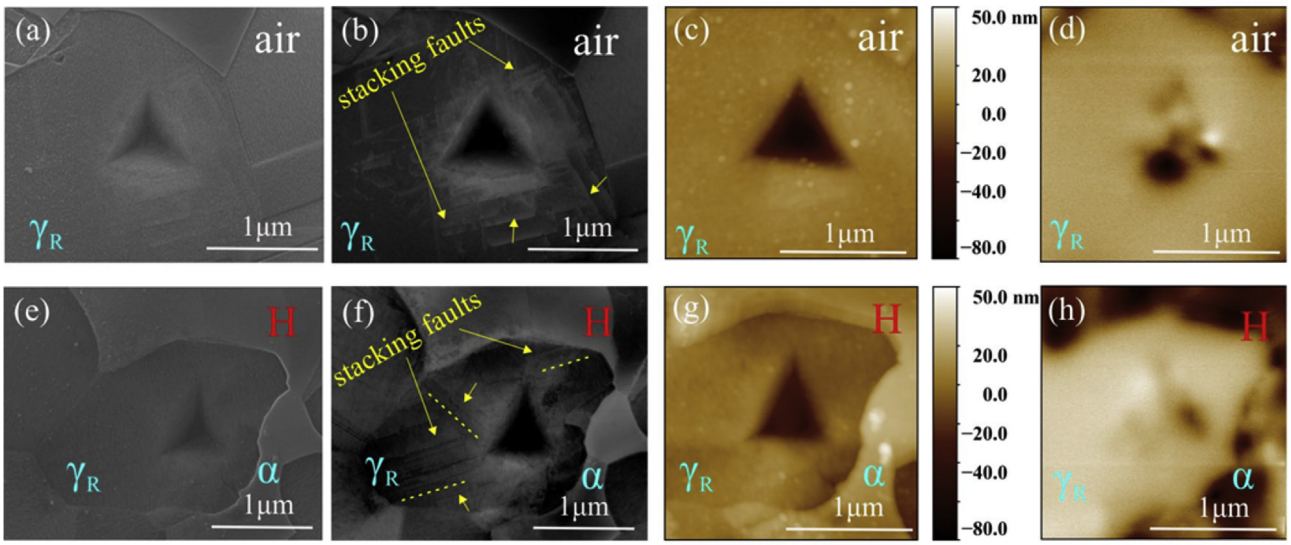

Fig. 4 – SEM (a), (e); ECC (b), (f); AFM (c), (g) and MFM (d), (h) images of austenite indents with and without hydrogen.

reason for this transition. However, in our study, the increment of hardness is reliable since we use a less sharp indenter according to Ref. [45] and a saturation layer of hydrogen test is guaranteed for the present charging condition.

Hydrogen effect on martensite phase transformation

To further study the effect of hydrogen on γ_R, electron channeling contrast imaging (ECCI) and magnetic force microscopy (MFM) techniques were applied to reveal the microstructure evolution and phase transformation. ECC images in Fig. 4 (b) shows that stacking faults were generated surrounding indent after nanomechanical loading in air. In contrast, more stacking faults showing planar mode in some certain directions can be observed during electrochemical charging, which are highlighted by yellow dot lines. The reduction of SFE in austenitic-base steels in a hydrogen-containing environment was previously studied by using in-situ transmission electron microscope (TEM) and X-ray diffraction (XRD) methods [26,47–49]. Further atomistic simulations proved this through hydrogen promotes partial dislocations separation and increases the energy needed for cross-slip [50]. Additionally, "Defactant" model based on thermodynamic consideration predicts a reduction of defects formation energy by introducing solute atoms, hydrogen for example [51]. Results shown in Fig. 4 (b) and (f) are consistent with the above-elaborated mechanisms. Fig. 4 (c) and (g) show topography images, and the corresponding MFM images exhibit clearly magnetic domain in ferrite. Interestingly, magnetic signals were also detected around austenite indents revealing austenite to α'-martensite transformation during the test. Albeit the stress-strain state may change due to different grain orientations, several different grains still showed consistent results revealing a stronger magnetic domain surrounding the air indents, which to some extent indicates a suppression of α'-martensite formation by introducing hydrogen. Nonetheless, it is reasonable to imply that the strain induced martensite transformation is highly influenced by the addition of hydrogen through the alteration of SFE and phase stability. Since the nucleation sites of α'-martensite are proposed to be the intersections of different slip systems, as revealed via TEM and MFM [52,53]. The reduced martensite transformation with the presence of hydrogen can, in some way, be explained by the following mechanism: the reduced SFE will promote slip planarity and hinder dislocations cross-slip, which unfavors the intersection of different slip systems that can locally increase the stress, and thus the nucleation of α'-martensite from those intersections are hindered. Hydrogen suppresses martensite transformation was reported in 316L stainless steel [52], where they observed a change of the dislocation structure from cellular to a mixture of cellular and planar mode. Although the reduction of martensite is expected to soften the material in the charged condition, it is not reflected on the current results. Further study on the influence of phase transformation on mechanical properties, especially hardness, is part of the planned experiments that will be performed in the future. This finding is indeed important, since transformation of austenite, which has high hydrogen solubility and low mobility, to α'-martensite, which has high hydrogen mobility and is prone to hydrogen embrittlement, can lead to pre-mature failure [54–56]. This study on the individual phase response upon hydrogen charging is dedicated to better understanding of the HE mechanisms in multiphase MMnS. Moreover, the results are promising to help understand the macroscale behavior of the material with hydrogen charging.

Conclusion

In summary, the hydrogen susceptibility of retained austenite and ferrite phases in a Fe-12Mn-3Al-0.05C (wt. %) medium-Mn steel was investigated by performing in-situ nanoindentation test in combination with SEM and MFM. Hydrogen was proposed to assist dislocation nucleation and reduced the stacking fault energy (SFE) of retained austenite. Strain-induced γ

Please cite this article as: Lu X et al., Insight into hydrogen effect on a duplex medium-Mn steel revealed by in-situ nanoindentation test, International Journal of Hydrogen Energy, https://doi.org/10.1016/j.ijhydene.2019.04.290

to α′-martensite transformation was to some extent suppressed in a hydrogen environment verified by MFM.

Acknowledgments

The authors gratefully acknowledge the financial support from the Research Council of Norway through the projects HyF-Lex (244068/E30), the Deutsche Forschungsgemeinschaft (DFG) within the Collaborative Research Center (SFB) 761 "Steel-ab initio: quantum mechanics guided design of new Fe based materials" and China Scholarship Council. Synchrotron X-ray diffraction experiment was carried out at beamline P02.1 of PETRA III, DESY (Hamburg, Germany), which is gratefully acknowledged. We would like to thank Rouven Schneider for performing MFM experiments.

REFERENCES

[1] He BB, Hu B, Yen HW, Cheng GJ, Wang ZK, Luo HW, et al. High dislocation density-induced large ductility in deformed and partitioned steels. Science 2017;357:1029–32. https://doi.org/10.1126/science.aan0177.
[2] Shi J, Sun XJ, Wang MQ, Hui WJ, Dong H, Cao WQ. Enhanced work-hardening behavior and mechanical properties in ultrafine-grained steels with large-fractioned metastable austenite. Scripta Mater 2010;63:815–8. https://doi.org/10.1016/j.scriptamat.2010.06.023.
[3] Arlazarov A, Goune M, Bouaziz O, Hazotte A, Petitgand G, Barges P. Evolution of microstructure and mechanical properties of medium Mn steels during double annealing. Mater Sci Eng A 2012;542:31–9. https://doi.org/10.1016/j.msea.2012.02.024.
[4] Ma Y. Medium-manganese steels processed by austenite-reverted-transformation annealing for automotive applications. Mater Sci Technol 2017;33:1713–27. https://doi.org/10.1080/02670836.2017.1312208.
[5] Suh DW, Kim SJ. Medium Mn transformation-induced plasticity steels: recent progress and challenges. Scripta Mater 2017;126:63–7. https://doi.org/10.1016/j.scriptamat.2016.07.013.
[6] De Cooman BC. 11 - high Mn TWIP steel and medium Mn steel. In: Rana R, Singh SB, editors. Automotive steels. Woodhead Publishing; 2017. p. 317–85.
[7] Li X, Song R, Zhou N, Li J. An ultrahigh strength and enhanced ductility cold-rolled medium-Mn steel treated by intercritical annealing. Scripta Mater 2018;154:30–3. https://doi.org/10.1016/j.scriptamat.2018.05.016.
[8] Hou ZR, Zhao XM, Zhang W, Liu HL, Yi HL. A medium manganese steel designed for water quenching and partitioning. Mater Sci Technol 2018;34:1168–75. https://doi.org/10.1080/02670836.2018.1426678.
[9] Galindo-Nava EI, Rivera-Diaz-del-Castillo PEJ. Understanding martensite and twin formation in austenitic steels: a model describing TRIP and TWIP effects. Acta Mater 2017;128:120–34. https://doi.org/10.1016/j.actamat.2017.02.004.
[10] He BB, Liang ZY, Huang MX. Nanoindentation investigation on the initiation of yield point phenomenon in a medium Mn steel. Scripta Mater 2018;150:134–8. https://doi.org/10.1016/j.scriptamat.2018.03.015.
[11] He BB, Huang MX. On the mechanical stability of austenite matrix after martensite formation in a medium Mn steel. Metall Mater Trans A 2016;47a:3346–53. https://doi.org/10.1007/s11661-016-3502-y.
[12] Koyama M, Akiyama E, Lee YK, Raabe D, Tsuzaki K. Overview of hydrogen embrittlement in high-Mn steels. Int J Hydrogen Energy 2017;42:12706–23. https://doi.org/10.1016/j.ijhydene.2017.02.214.
[13] Dwivedi SK, Vishwakarma M. Hydrogen embrittlement in different materials: a review. Int J Hydrogen Energy 2018;43:21603–16. https://doi.org/10.1016/j.ijhydene.2018.09.201.
[14] Wang YF, Gong JM, Jiang WC. A quantitative description on fracture toughness of steels in hydrogen gas. Int J Hydrogen Energy 2013;38:12503–8. https://doi.org/10.1016/j.ijhydene.2013.07.033.
[15] da Silva BRS, Salvio F, dos Santos DS. Hydrogen induced stress cracking in UNS S32750 super duplex stainless steel tube weld joint. Int J Hydrogen Energy 2015;40:17091–101. https://doi.org/10.1016/j.ijhydene.2015.08.028.
[16] Villalobos JC, Serna SA, Campillo B, Lopez-Martinez E. Evaluation of mechanical properties of an experimental microalloyed steel subjected to tempering heat treatment and its effect on hydrogen embrittlement. Int J Hydrogen Energy 2017;42:689–98. https://doi.org/10.1016/j.ijhydene.2016.10.103.
[17] Xing X, Chen WX, Zhang H. Atomistic study of hydrogen embrittlement during cyclic loading: quantitative model of hydrogen accumulation effects. Int J Hydrogen Energy 2017;42:4571–8. https://doi.org/10.1016/j.ijhydene.2016.12.127.
[18] Garcia DCS, Carvalho RN, Lins VFC, Rezende DM, Dos Santos DS. Influence of microstructure in the hydrogen permeation in martensitic-ferritic stainless steel. Int J Hydrogen Energy 2015;40:17102–9. https://doi.org/10.1016/j.ijhydene.2015.06.102.
[19] Gan LJ, Huang F, Zhao XY, Liu J, Cheng YF. Hydrogen trapping and hydrogen induced cracking of welded X100 pipeline steel in H2S environments. Int J Hydrogen Energy 2018;43:2293–306. https://doi.org/10.1016/j.ijhydene.2017.11.155.
[20] Ornek C, Reccagni P, Kivisakk U, Bettini E, Engelberg DL, Pan JS. Hydrogen embrittlement of super duplex stainless steel - towards understanding the effects of microstructure and strain. Int J Hydrogen Energy 2018;43:12543–55. https://doi.org/10.1016/j.ijhydene.2018.05.028.
[21] Gerberich WW, Nelson JC, Lilleodden ET, Anderson P, Wyrobek JT. Indentation induced dislocation nucleation: the initial yield point. Acta Mater 1996;44:3585–98. https://doi.org/10.1016/1359-6454(96)00010-9.
[22] Bahr DF, Kramer DE, Gerberich WW. Non-linear deformation mechanisms during nanoindentation. Acta Mater 1998;46:3605–17. https://doi.org/10.1016/S1359-6454(98)00024-X.
[23] Dehm G, Jaya BN, Raghavan R, Kirchlechner C. Overview on micro- and nanomechanical testing: new insights in interface plasticity and fracture at small length scales. Acta Mater 2018;142:248–82. https://doi.org/10.1016/j.actamat.2017.06.019.
[24] Barnoush A. Correlation between dislocation density and nanomechanical response during nanoindentation. Acta Mater 2012;60:1268–77. https://doi.org/10.1016/j.actamat.2011.11.034.
[25] Barnoush A, Vehoff H. Electrochemical nanoindentation: a new approach to probe hydrogen/deformation interaction. Scripta Mater 2006;55:195–8. https://doi.org/10.1016/j.scriptamat.2006.03.041.
[26] Barnoush A, Vehoff H. Recent developments in the study of hydrogen embrittlement: hydrogen effect on dislocation nucleation. Acta Mater 2010;58:5274–85. https://doi.org/10.1016/j.actamat.2010.05.057.

Please cite this article as: Lu X et al., Insight into hydrogen effect on a duplex medium-Mn steel revealed by in-situ nanoindentation test, International Journal of Hydrogen Energy, https://doi.org/10.1016/j.ijhydene.2019.04.290

[27] Ma Y, Song WW, Zhou SX, Schwedt A, Bleck W. Influence of intercritical annealing temperature on microstructure and mechanical properties of a cold-rolled medium-Mn steel. Metals 2018;8. https://doi.org/10.3390/met8050357.
[28] Lutterotti L. Total pattern fitting for the combined size-strain-stress-texture determination in thin film diffraction. Nucl Instrum Methods Phys Res, Sect B 2010;268:334–40. https://doi.org/10.1016/j.nimb.2009.09.053.
[29] Stenerud G, Johnsen R, Olsen JS, He JY, Barnoush A. Effect of hydrogen on dislocation nucleation in alloy 718. Int J Hydrogen Energy 2017;42:15933–42. https://doi.org/10.1016/j.ijhydene.2017.04.290.
[30] Wang D, Lu X, Deng Y, Guo X, Barnoush A. Effect of hydrogen on nanomechanical properties in Fe-22Mn-0.6C TWIP steel revealed by in-situ electrochemical nanoindentation. Acta Mater 2019;166:618–29. https://doi.org/10.1016/j.actamat.2018.12.055.
[31] Luo HW, Dong H, Huang MX. Effect of intercritical annealing on the Luders strains of medium Mn transformation-induced plasticity steels. Mater Des 2015;83:42–8. https://doi.org/10.1016/j.matdes.2015.05.085.
[32] Han QH, Zhang YL, Wang L. Effect of annealing time on microstructural evolution and deformation characteristics in 10Mn1.5Al TRIP steel. Metall Mater Trans A 2015;46a:1917–26. https://doi.org/10.1007/s11661-015-2822-7.
[33] Suresh S, Nieh TG, Choi BW. Nano-indentation of copper thin films on silicon substrates. Scripta Mater 1999;41:951–7. https://doi.org/10.1016/S1359-6462(99)00245-6.
[34] Gouldstone A, Koh HJ, Zeng KY, Giannakopoulos AE, Suresh S. Discrete and continuous deformation during nanoindentation of thin films. Acta Mater 2000;48:2277–95. https://doi.org/10.1016/j.actamat.2017.02.004.
[35] Lorenz D, Zeckzer A, Hilpert U, Grau P, Johansen H, Leipner HS. Pop-in effect as homogeneous nucleation of dislocations during nanoindentation. Phys Rev B 2003;67. https://doi.org/10.1103/PhysRevB.67.172101.
[36] He BB, Huang MX, Liang ZY, Ngan AHW, Luo HW, Shi J, et al. Nanoindentation investigation on the mechanical stability of individual austenite grains in a medium-Mn transformation-induced plasticity steel. Scripta Mater 2013;69:215–8. https://doi.org/10.1016/j.scriptamat.2013.03.030.
[37] Misra RDK, Zhang Z, Jia Z, Somani MC, Karjalainen LP. Probing deformation processes in near-defect free volume in high strength high ductility nanograined/ultrafine-grained (NG/UFG) metastable austenitic stainless steels. Scripta Mater 2010;63:1057–60. https://doi.org/10.1016/j.scriptamat.2010.07.041.
[38] Schuh CA, Lund AC. Application of nucleation theory to the rate dependence of incipient plasticity during nanoindentation. J Mater Res 2004;19:2152–8. https://doi.org/10.1557/JMR.2004.0276.
[39] Schuh CA, Mason JK, Lund AC. Quantitative insight into dislocation nucleation from high-temperature nanoindentation experiments. Nat Mater 2005;4:617–21. https://doi.org/10.1038/nmat1429.
[40] Johnson KL. Contact mechanics. Cambridge: Cambridge University Press; 1985.
[41] Yang G, Zhao Y, Lee DH, Park JM, Seok MY, Suh JY, et al. Influence of hydrogen on incipient plasticity in CoCrFeMnNi high-entropy alloy. Scripta Mater 2019;161:23–7. https://doi.org/10.1016/j.scriptamat.2018.10.010.
[42] Nibur KA, Bahr DF, Somerday BP. Hydrogen effects on dislocation activity in austenitic stainless steel. Acta Mater 2006;54:2677–84. https://doi.org/10.1016/j.actamat.2006.02.007.
[43] Kheradmand N, Johnsen R, Olsen JS, Barnoush A. Effect of hydrogen on the hardness of different phases in super duplex stainless steel. Int J Hydrogen Energy 2016;41:704–12. https://doi.org/10.1016/j.ijhydene.2015.10.106.
[44] Barnoush A, Asgari M, Johnsen R. Resolving the hydrogen effect on dislocation nucleation and mobility by electrochemical nanoindentation. Scripta Mater 2012;66:414–7. https://doi.org/10.1016/j.scriptamat.2011.12.004.
[45] Lee DH, Lee JA, Seok MY, Baek UB, Nahm SH, Jang JI. Stress-dependent hardening-to-softening transition of hydrogen effects in nanoindentation of a linepipe steel. Int J Hydrogen Energy 2014;39:1897–902. https://doi.org/10.1016/j.ijhydene.2013.11.060.
[46] Zhao YK, Seok MY, Choi IC, Lee YH, Park SJ, Ramamurty U, et al. The role of hydrogen in hardening/softening steel: influence of the charging process. Scripta Mater 2015;107:46–9. https://doi.org/10.1016/j.scriptamat.2015.05.017.
[47] Ferreira PJ, Robertson IM, Birnbaum HK. Influence of hydrogen on the stacking-fault energy of an austenitic stainless steel. Mater Sci Forum 1996;207–209:93–6. https://doi.org/10.4028/www.scientific.net/MSF.207-209.93.
[48] Hermida JD, Roviglione A. Stacking fault energy decrease in austenitic stainless steels induced by hydrogen pairs formation. Scripta Mater 1998;39:1145–9. https://doi.org/10.1016/S1359-6462(98)00285-1.
[49] Pontini AE, Hermida JD. X-ray diffraction measurement of the stacking fault energy reduction induced by hydrogen in an AISI 304 steel. Scripta Mater 1997;37:1831–7. https://doi.org/10.1016/S1359-6462(97)00332-1.
[50] Wen M, Fukuyama S, Yokogawa K. Atomistic simulations of hydrogen effect on dissociation of screw dislocations in nickel. Scripta Mater 2005;52:959–62. https://doi.org/10.1016/j.scriptamat.2005.01.044.
[51] Kirchheim R. Reducing grain boundary, dislocation line and vacancy formation energies by solute segregation. I. Theoretical background. Acta Mater 2007;55:5129–38. https://doi.org/10.1016/j.actamat.2007.05.047.
[52] Bak SH, Kim SS, Lee DB. Effect of hydrogen on dislocation structure and strain-induced martensite transformation in 316L stainless steel. RSC Adv 2017;7:27840–5. https://doi.org/10.1039/C7RA01053B.
[53] Mine Y, Horita Z, Murakami Y. Effect of hydrogen on martensite formation in austenitic stainless steels in high-pressure torsion. Acta Mater 2009;57:2993–3002. https://doi.org/10.1016/j.actamat.2009.03.006.
[54] Han J, Nam JH, Lee YK. The mechanism of hydrogen embrittlement in intercritically annealed medium Mn TRIP steel. Acta Mater 2016;113:1–10. https://doi.org/10.1016/j.actamat.2016.04.038.
[55] Ryu JH, Chun YS, Lee CS, Bhadeshia HKDH, Suh DW. Effect of deformation on hydrogen trapping and effusion in TRIP-assisted steel. Acta Mater 2012;60:4085–92. https://doi.org/10.1016/j.actamat.2012.04.010.
[56] Zhang L, Li ZY, Zheng JY, Zhao YZ, Xu P, Zhou CL, et al. Effect of strain-induced martensite on hydrogen embrittlement of austenitic stainless steels investigated by combined tension and hydrogen release methods. Int J Hydrogen Energy 2013;38:8208–14. https://doi.org/10.1016/j.ijhydene.2013.01.198.

Please cite this article as: Lu X et al., Insight into hydrogen effect on a duplex medium-Mn steel revealed by in-situ nanoindentation test, International Journal of Hydrogen Energy, https://doi.org/10.1016/j.ijhydene.2019.04.290